

ALTERED MITOCHONDRIAL DYNAMICS IN VENEZUELAN EQUINE
ENCEPHALITIS VIRUS INFECTED CELLS

by

Taryn Brooks-Faulconer
A Thesis
Submitted to the
Graduate Faculty
of
George Mason University
in Partial Fulfillment of
The Requirements for the Degree
of
Master of Science
Biology

Committee:

_____ Dr. Aarthi Narayanan
Thesis Director

_____ Dr. Kylene Kehn-Hall
Committee Member

_____ Dr. Ancha Baranova
Committee Member

_____ Dr. Iosif Vaisman
Acting Director, School of Systems Biology

_____ Dr. Donna M. Fox
Associate Dean, Office of Student Affairs &
Special Programs

_____ Dr. Peggy Agouris
Dean, College of Science

Date: _____ Spring Semester 2016
George Mason University
Fairfax, VA

Altered Mitochondrial Dynamics in Venezuelan Equine Encephalitis Virus Infected Cells

A Thesis submitted in partial fulfillment of the requirements for the degree of Master of Science at George Mason University

by

Taryn Brooks-Faulconer
Bachelor of Science
George Mason University, 2014

Director: Aarthi Narayanan, Professor
School of Systems Biology

Spring Semester 2016
George Mason University
Fairfax, VA



This work is licensed under a [creative commons attribution-noncommercial 3.0 unported license](https://creativecommons.org/licenses/by-nc/3.0/).

DEDICATION

This is dedicated to my husband, David, my children, Kathryn, Christopher, Tamara and Amanda, and especially my mother, Catherine, who has taught me to persevere in the face of any obstacle that might fall in one's path along the road of life.

ACKNOWLEDGEMENTS

I would like to thank the many supporters who have made this thesis happen. My principal investigator, Dr. Aarthi Narayanan, consistently encouraged me to exceed even my own expectations. Dr. Moushimi Amaya, whose patient willingness to share her expertise was invaluable to my ability to grasp concepts and acquire the research skills needed to complete the work. Dr. Larry Rockwood for awarding me a graduate teaching assistantship in my first semester, enabling me to start my journey toward a research and teaching career from the get-go. Drs. Kehn-Hall, Wu, Van Hoek and Baranova, all of whom provided positive encouragement along the way. Finally I would like to thank all of my friends and professors at George Mason University, who accompanied me on my journey through two bachelor's degrees and two years as a master's student. I could not have done this alone.

TABLE OF CONTENTS

| | Page |
|---|------|
| List of Figures | vii |
| List of Abbreviations And Symbols | viii |
| Abstract | x |
| Chapter One: Introduction | 1 |
| Venezuelan Equine Encephalitis Virus | 1 |
| Mitochondrial Dynamics in Viral Infections | 2 |
| Chapter Two: Materials and Methods..... | 7 |
| Viruses and Cell Lines | 7 |
| Viral Infections..... | 7 |
| TMRE Assay | 7 |
| Reactive Oxygen Species Detection | 8 |
| Reactive Oxygen Species Quantitation | 8 |
| Immunofluorescence | 9 |
| Mitochondrial Extraction | 9 |
| Western Blot Analysis..... | 10 |
| Transfections and Protein Extracts..... | 10 |
| Electron Microscopy Analysis | 11 |
| Statistical Analysis | 11 |
| Chapter Three: Results..... | 13 |
| VEEV infection results in loss of mitochondrial membrane potential and increase in reactive oxygen species | 13 |
| Infected cells displayed differences in intracellular mitochondrial location in comparison with uninfected cells..... | 17 |
| The VEEV capsid protein was observed to localize in the mitochondria. | 18 |
| VEEV capsid co-localized with PINK1 and Parkin in the mitochondrial membrane of TC-83 infected cells. | 22 |

| | |
|--|----|
| Overexpression of capsid protein resulted in a decrease in mitochondrial membrane potential and altered intracellular distribution. | 26 |
| High resolution imaging of VEEV infected cells demonstrated alterations in mitochondrial structure. | 28 |
| Chapter Four: Discussion..... | 30 |
| References..... | 36 |

LIST OF FIGURES

| Figure | Page |
|---|------|
| Figure 1 TC-83 infection of U87MG cells resulted in loss of membrane potential and an increase in reactive oxygen species. | 16 |
| Figure 2 Mitochondria displayed a perinuclear phenotype in TC-83 infected cells. | 18 |
| Figure 3 VEEV capsid localized in the mitochondria of infected cells. | 20 |
| Figure 4 VEEV capsid localized to the mitochondrial membranes of infected cells in an infection dependent manner. | 21 |
| Figure 5 VEEV capsid co-localized with PINK1 and Parkin. | 23 |
| Figure 6 PINK1 and Parkin co-localize in the mitochondrial membrane of TC-83 infected cells. | 25 |
| Figure 7 Over expressed VEEV capsid resulted in altered mitochondrial dynamics. | 27 |
| Figure 8 Mitochondria in TC-83 infected cells display morphological alterations. | 29 |

LIST OF ABBREVIATIONS AND SYMBOLS

| | |
|---|------------------|
| 2-(N-morpholino) ethanesulfonic acid..... | MES |
| 2', 7'-Dichlorodihydrofluorescein..... | DCF |
| 2', 7'-Dichlorodihydrofluorescein diacetate..... | DCFH-DA |
| 4',6-diamindino-2-phenylindole fluorescent nuclear stain..... | DAPI |
| Adenosine triphosphate..... | ATP |
| Beta-actin protein..... | β -actin |
| Carbon dioxide..... | CO ₂ |
| Carbonyl cyanide 4-(trifluoromethoxy) phenylhydrazine..... | FCCP |
| Cytopathic Effect..... | CPE |
| Degrees Celsius..... | °C |
| Deoxyribose nucleic acid..... | DNA |
| Dulbecco's Modified Eagle Medium..... | DMEM |
| Eastern Equine Encephalitis Virus..... | EEEV |
| Envelope protein 2..... | E2 |
| Extracellular-signal-regulated kinase..... | ERK |
| Fetal Bovine Serum..... | FBS |
| Food and Drug Administration..... | FDA |
| Green Fluorescent Protein..... | GFP |
| Hepatitis B Virus..... | HBV |
| Hepatitis B Virus Protein X..... | HBVx |
| Hepatitis C Virus..... | HCV |
| Horseradish peroxidase..... | HRP |
| Hours post infection..... | hpi |
| Human Immunodeficiency Virus..... | HIV |
| Human glioblastoma-astrocytoma cell line..... | U87MG |
| Microliter..... | μ L |
| Micromolar..... | μ M |
| Milliliter..... | mL |
| Mitochondrial antiviral signaling protein..... | MAVS |
| Mitogen-activated protein kinase kinase..... | MEK |
| Molar..... | M |
| Multiplicity of infection..... | MOI |
| Nonstructural protein 1..... | NS1 |
| Nonstructural protein m..... | NSm |
| Nonstructural S protein..... | NSs |
| Osmiumtetroxide..... | OsO ₄ |

| | |
|--|----------|
| Overnight incubation | ON |
| Phosphate-buffered saline | PBS |
| Polyvinylidene fluoride..... | PVDF |
| Potassiumferrocyanide | KFeCN6 |
| PTEN-induced putative kinase 1 | PINK1 |
| Ribonucleic acid..... | RNA |
| Rift Valley Fever Virus..... | RVFV |
| Reactive Oxygen Species..... | ROS |
| Respiratory Syncytial Virus..... | RSV |
| Retinoic acid-inducible gene 1..... | RIG-I |
| Room Temperature | RT |
| Sodium dodecyl sulfate polyacrylamide gel electrophoresis | SDS-PAGE |
| TetraMethyl Rhodamine, Ethyl ester | TMRE |
| Tissue Protein Extraction Reagent..... | T-PER |
| Translocon of outer mitochondrial membrane 20 protein | TOMM20 |
| Transmission Electron Microscopy | TEM |
| Venezuelan Equine Encephalitis Virus..... | VEEV |
| Venezuelan Equine Encephalitis Virus Attenuated Vaccine | TC-83 |
| Venezuelan Equine Encephalitis Virus Formalin-Inactivated Vaccine..... | C-84 |
| Venezuelan Equine Encephalitis Virus Virulent Trinidad Donkey Strain | TrD |
| Viral Protein R | Vpr |
| Western Equine Encephalitis Virus | WEEV |
| Whole cell extract | WCE |

ABSTRACT

ALTERED MITOCHONDRIAL DYNAMICS IN VENEZUELAN EQUINE ENCEPHALITIS VIRUS INFECTED CELLS

Taryn Brooks-Faulconer, M.S.

George Mason University, 2016

Thesis Director: Dr. Aarthi Narayanan

To establish productive infection, viruses profoundly alter both the intracellular environment and the cellular function. Mitochondria are critically important cellular organelles that generate energy and ensure cell survival. Mitochondria are also crucial for innate immunity response as they serve as the sentinels that sense infection and initiate host responses. For many viruses, the changes in mitochondrial dynamics were documented to occur early in infection. Venezuelan Equine Encephalitis Virus (VEEV) is a New World alphavirus that infects neuronal cells and produces an encephalitic phenotype. In this manuscript, we demonstrate that VEEV infection results in mitochondrial alterations that include changes in the morphology and intracellular distribution of mitochondria, reduction in mitochondrial membrane potential and localization of their enzymatic components. In particular, we report perinuclear accumulation of mitochondria in infected cells and partial co-localization of the viral

capsid proteins with mitochondrial membranes. The pronounced changes to the mitochondria observed in VEEV infected cells probably play a role in the development of the virus-specific cytopathic effects. Our studies demonstrate that the mitochondria are critical intracellular platforms affected by alphavirus infections.

CHAPTER ONE: INTRODUCTION

Venezuelan Equine Encephalitis Virus

Venezuelan Equine Encephalitis Virus (VEEV) is a single-stranded RNA virus of the genus *Alphavirus*, family *Togaviridae*. VEEV is an emerging infectious agent that causes natural outbreaks in many parts of the world, with a significant recent outbreak recorded in 2013 in South America (Weaver, 2005; Taylor and Paessler, 2013). Due to the retention of stability and infectivity in the aerosol form, VEEV was weaponized in the past and continues to be classified as a bio-threat agent and category B select agent. This virus is also considered to be a re-emerging pathogen, since following a 19 year period with no reported cases of VEEV infection, in the past decade outbreaks have occurred in Mexico, and North, Central and South America (Weaver et al., 2004). In fact, a 1995 reemergence of VEEV in Venezuela and Colombia led to 75,000 – 100,000 known human cases (Weaver et al., 1996).

New World alphaviruses include, in addition to VEEV, Eastern Equine Encephalitis Virus (EEEV) and Western Equine Encephalitis Virus (WEEV), which also infect humans. EEEV infections result in the highest mortality (70%), while VEEV infections in children and younger populations are more harmful (~25% mortality) than in the case of adults (1% mortality). New World alphaviruses infect both equines and humans in natural settings. Equines typically develop generalized symptoms within 2-5

days of VEEV infection, including fever, tachycardia, depression, and anorexia. More serious complications, including hyperexcitability and encephalitis sometimes occur within 5-10 days of infection, often resulting in death of the animal within one week. When humans are infected with VEEV, symptoms appear within 2-5 days and range from febrile, or flu-like symptoms, such as malaise, fever, chills and myalgia, to coma and death that are registered in ~1% of cases. Currently, no FDA approved vaccines or therapeutics are available for VEEV infection treatment. However, there are two investigational vaccines for VEEV that are offered by the U.S. Army to at-risk personnel (Paessler and Weaver, 2009). These include VEEV TC-83 strain, which is a live-attenuated virus known to induce a fairly robust primary immune response, and C-84, which is a formalin-inactivated vaccine that induces only weak immune responses. The use of TC-83 is associated with considerable safety concerns due to its reactogenicity; hence, it is not approved as a vaccine for the general population. TC-83 is used as a vaccination for equines, military and at-risk personnel, while the inactivated trivalent encephalitic virus vaccine (VEEV, EEEV and WEEV) is more commonly used in horses (Barber et al., 1978; Amaya et al., 2015).

Mitochondrial Dynamics in Viral Infections

The role of mitochondrial dynamics during acute viral infections is beginning to be appreciated. Mitochondria are central to many cellular processes, including energy production, aging, innate immunity and cell survival (Ernster and Schatz, 1981; Chan, 2006; McBride et al., 2006; Khan et al., 2015). Mitochondrial size, structure and motility influence cellular homeostasis as it has been demonstrated in the case of

neurodegenerative disorders including Parkinson's, Alzheimer's and Huntington's diseases (Detmer and Chan, 2007; Su et al., 2010).

The list of viruses that impact mitochondria and innate immune responses is growing. Many viral proteins target the mitochondria and interfere with their functionality. For example, the hepatitis B virus (HBV), a DNA virus in the *Hepadnaviridae* family, encodes regulatory protein HBV X (HBx) that localizes to the mitochondrial membrane, where it alters membrane potential, and elevates the levels of calcium ions and the production of Reactive Oxygen Species (ROS), thereby causing damage to the mitochondria (Rahmani et al., 2000; Bouchard et al., 2001; Waris et al., 2001; Bouchard and Navas-Martin, 2011). Similarly, Hepatitis C virus (HCV), a positive-strand RNA virus in the *Flaviviridae* family, has also been shown to damage the mitochondria in the liver due to an increase in the production of ROS resulting in membrane depolarization and dysfunction (Bouchard and Navas-Martin, 2011). HCV infection also induces a perinuclear phenotype, wherein mitochondria cluster in the perinuclear space (Kim et al., 2013). In addition, HCV infection induces the changes in the mitochondrial membrane proteome, and the mitochondrial localization of the kinase PINK1 and the ubiquitin ligase Parkin (Kim et al., 2013; Kim et al., 2014).

PINK1 and Parkin are important quality control proteins that are involved in the maintenance of mitochondrial homeostasis (Khan et al., 2014). In fact, PINK1 deficiency has been shown to impair mitochondrial calcium efflux, inhibit glucose uptake and increase ROS in neuronal cells (Gandhi et al., 2009). However, the mechanism which underlies homeostatic control of PINK1 is unknown (Okatsu et al., 2012). In healthy

mitochondria, newly synthesized PINK1 is imported to the inner membrane, where it undergoes protease-dependent cleavage of its N-terminal domain and is subsequently degraded by the proteasome (Okatsu et al., 2012). When mitochondria are damaged by physiological stress, including viral infections, PINK1 is translocated from the outer membrane to the inner mitochondrial membrane where it selectively flags impaired portions that have undergone fission by the dynamin-related protein DRP-1. This facilitates Parkin recruitment to the mitochondrial membrane and leads to mitophagy of the damaged portions, while healthy portions are recruited to the mitochondrial network and repaired by fusion with other healthy segments (Okatsu et al., 2012; Khan et al., 2014). If the processes of fission and fusion are not in balance, then apoptosis may occur from either excessive fission and/or insufficient fusion (Suen et al., 2008). For instance, an accumulation of DRP-1 can increase the rate of fission and the fragmentation of mitochondria, inducing apoptosis. In addition, inhibition of at least one of two key fusion proteins, mitofusin 1 (Mfn1) or mitofusin 2 (Mfn2), may also lead to an increase in fragmentation and susceptibility of apoptosis. Conversely, overexpression of either of these fusion proteins can lead to a delay in Bax activation, cytochrome c release, caspase activation and cell death (Suen et al., 2008). In turn, alterations of the spatial distribution of enzymes may influence their posttranslational modifications and activity.

As another example, the viral protein Vpr, from the retrovirus HIV is associated with the mitochondrial outer membrane. It decreases the expression of Mfn2, leading to mitochondrial fragmentation, which ultimately affects T lymphocyte viability. The negative-stranded RNA virus Respiratory Syncytial Virus (RSV) in the family

Paramyxoviridae encodes a nonstructural protein 1 (NS1) that interferes with antiviral signaling originating from the mitochondria (Boyapalle et al., 2012). The virulence factor NSs of Rift Valley fever virus (RVFV), a negative-stranded RNA virus in the family *Bunyaviridae*, associates with the mitochondria and disrupts the redox balance of the cell, leading to apoptosis (Narayanan et al., 2014). The RVFV NSm protein that is associated with onset of apoptosis in infected cells has also been shown to localize to mitochondria (Terasaki et al., 2013).

In the case of New World alphaviruses, infection is known to cause lethal outcomes with cytopathic effects in neuronal cells (Garmashova et al., 2007; Atasheva et al., 2010; Atasheva et al., 2015). The mechanisms that underlie virus-induced neuronal death are not clear. Only a few studies proceed beyond the measurements of the caspase activation in a manner that is dependent on infection. In the case of VEEV, these cytopathic effects (CPE) have been demonstrated to involve capsid protein-dependent inhibition of host cellular transcription. Specifically, this transcriptional shutoff is effected by a short peptide, C_{vee}33-68, on the N-terminal region of the capsid protein, which interacts with the nuclear pore complex (NPC) (Garmashova et al., 2007). VEEV capsid protein forms a tetrameric complex with importin α/β and CRM1 that associates with the NPC and interferes with its functioning. Capsid also has a nuclear localization signal (NLS) and nuclear export signal (NES) that allow interaction with the NPC through association with host proteins. It is likely that these features induce inhibition of host cellular transcription and lead to the CPE observed in VEEV infected cells (Atasheva et al., 2010; Lundberg et al., 2013).

Thus far, the field of New World alphaviruses has not focused on the mitochondria, hence, the influence of alphaviral infections on mitochondrial dynamics remains unknown. Our studies were initiated in order to test the hypothesis that VEEV infection results in alteration of mitochondrial dynamics and disruption of membrane potential. We additionally hypothesize that in infected cells mitochondria change their intracellular distribution and proteome composition.

To address the impact of VEEV infection on the mitochondria of infected cells, we adopted a combination research strategy that included biochemical analysis of mitochondrial membrane potential and mitochondrial membrane protein composition. Confocal and electron microscopic methods were utilized to study the localization of host and viral components within the mitochondria and the alterations in mitochondrial structure, respectively. Our studies indicate that VEEV infection, indeed, disrupts mitochondrial structure and function. At least in part, this disruption may be explained by the integration of viral capsid proteins into the mitochondrial membrane. The results of this study help to understand the role of the changes in mitochondria in the progression of viral disease and the neuronal outcomes in VEEV infection.

CHAPTER TWO: MATERIALS AND METHODS

Viruses and Cell Lines

The live-attenuated virus TC-83 used in this study was obtained from BEI resources. Eighty-three passages of the virulent IAB Trinidad donkey (TrD) strain in guinea pig heart cells resulted in the TC-83 virus (Johnson et al., 1986; Kinney et al., 1989). TC-83 attenuation has been mapped to changes in the 5'-noncoding region and the E2 envelope glycoprotein (Kinney et al., 1993). Human astrocytoma cells U87MG were maintained in DMEM supplemented with 10% Fetal Bovine Serum (FBS), 1% Penicillin/Streptomycin, and 1% L-Glutamine at 37°C and 5% CO₂.

Viral Infections

Cells were seeded in either a 96-well plate or an 8-well chamber slide, in order to attain confluency within 24 hours. The media was removed and the cells were infected for 1 hour to allow for viral adsorption at 37°C. The viral inoculum was then removed and replaced with complete medium. The cells were incubated at 37°C, 5% CO₂ for the time period indicated in each experiment.

TMRE Assay

TMRE-Mitochondrial Membrane Potential Assay Kit was obtained from Abcam Inc., Cambridge MA (Cat #ab113852). U87MG cells were seeded in a 96-well black plate at a density of 10,000 cells per well. Cells were either uninfected (Mock) or infected with TC-83 (MOI: 10 and MOI: 20). As a positive control, FCCP (50µM) diluted in

complete medium was added to mock cells and incubated at 37°C for 15 minutes. At 2, 4 and 6 hours post infection (hpi) the media was removed and cells were treated with 1µM TMRE (TetraMethyl Rhodamine, Ethyl ester) reagent diluted in complete medium. After 20 minutes incubation at 37°C, fluorescence was detected using the DTX 880 multimode detector (Beckman Coulter).

Reactive Oxygen Species Detection

To detect ROS in infected cells, U87MG cells were seeded at 20,000 cells per well in an eight-chamber slide. The slides were incubated at 37°C, 5% CO₂ overnight and infected with TC-83. At appropriate time points following infection, MitoSox reagent (Invitrogen, Cat#M36008) was added according to manufacturer's instructions and as described in (Narayanan et al., 2011). Cells were imaged using Nikon Eclipse TE2000-U.

Reactive Oxygen Species Quantitation

ROS levels were determined using OxiSelect Intracellular ROS Assay Kit (Cell Biolabs Inc., San Diego, CA, USA), according to the manufacturer's instructions. Briefly, ROS species react with 2',7'-dichlorodihydrofluorescein (DCFH-DA), which is rapidly oxidized to the fluorescent DCF. Its fluorescence intensity is proportional to the total ROS levels within the cell cytosol. U87MG cells were seeded in a 96-well black plate and were either uninfected (mock), infected with TC-83 MOI: 10, or treated with 100µM H₂O₂. Cells were pre-incubated for 30 minutes with 1X (1M) DCFH-DA in FBS-free DMEM prior to infection/treatment for 1 hour at 37°C, 5% CO₂. The addition of H₂O₂ to uninfected cells served as a positive control and uninfected mock cells served as a

negative control. Fluorescence was detected at 6 hpi using the DTX 880 multimode detector (Beckman Coulter).

Immunofluorescence

U87MG cells were seeded at a density of 20,000 cells per well in an 8-well chamber slide. The cells were either uninfected (Mock) or infected with TC-83 or transfected with VEEV-GFP-Capsid (Lundberg et al., 2013). At appropriate time points, the cells were fixed with 4% paraformaldehyde for 20 minutes and permeabilized with 0.5% Triton X-100 in PBS for 15 minutes. Slides were washed with PBS and blocked at room temperature for 10 minutes with 3% BSA. The slides were incubated with primary antibody VEEV Capsid (BEI Resources, NR-9403), TOMM20 (Abcam, ab78547), PINK1 (Santa Cruz Biotechnology, sc-33798), Parkin (Santa Cruz Biotechnology, sc-30130) for 1 hour at room temperature. The samples were then washed three times with PBS and incubated with respective secondary antibody Alexa Fluor antibodies (Invitrogen) for 1 hour in the dark at room temperature. Slides were washed three times with PBS and mounted with DAPI Fluoromount-G (SouthernBiotech, Catalogue No. 0100-20) and stored in the dark, at 4°C overnight. The cells were imaged using Nikon Eclipse TE2000-U using the 60x objective.

Mitochondrial Extraction

Mitochondrial membrane and cytosolic fractions were obtained using the Mitochondrial Extraction Kit for Cultured Cells (Thermo Scientific, #89874) according to the manufacturer's instructions. Briefly, U87MG cells were infected with TC-83 and collected at 6 hpi. Mitochondrial membrane and cytosolic fractions were isolated by

incubating sequentially with three proprietary reagents (A-C). Following incubation with reagent C, the cells were centrifuged for 10 minutes at 700 X g and the pellet was separated and discarded. The supernatant was then centrifuged again at 12,000 X g for 15 minutes, which will result in the separation of the mitochondria from the cytosol. Following a final wash with reagent C, the mitochondrial pellet was obtained by centrifuging the sample at 12,000 X g for 5 minutes. The pellet was resuspended in Laemmli buffer before being subjected to SDS-PAGE.

Western Blot Analysis

Whole cell and fractionated lysates were separated on a 4-20% Tris-Glycine Gel and transferred to a polyvinyl difluoride (PVDF) membrane using the iBlot gel transfer system (Invitrogen). Membranes were incubated with primary antibodies to VEEV Capsid, TOMM20, PINK1, or Parkin at 4°C overnight in 1% milk. The blots were incubated with appropriate secondary HRP-coupled antibody for 2 hours at room temperature. The membranes were visualized by chemiluminescence using SuperSignal West Femto Maximum Sensitivity Substrate Kit (ThermoScientific) and a BIO-RAD Molecular Imager ChemiDoc XRS system (BIO-RAD).

Transfections and Protein Extracts

Transfections were performed using Attractene Transfection Reagent (Qiagen, Catalogue No. 301005) as per the manufacturer's instructions and cells were processed after 24 hours incubation at 37°, 5% CO₂. For the preparation of whole cell lysates, the media was removed and the cells washed twice with PBS. The cells were lysed with lysis buffer that consisted of a 1:1 mixture of T-PER reagent (Pierce, Catalogue No. 78510),

Tris-glycine SDS sample buffer (Invitrogen, Catalogue No. LC2676), 2.5% β -mercaptoethanol, and protease/phosphatase inhibitor cocktail (1x Halt mixture, Pierce). The cell lysates were boiled for 10 minutes and stored at -80°C until analyzed.

Electron Microscopy Analysis

After infection, samples were washed three times with 0.5M MES buffer. Subsequently, samples were fixed with 2.5% glutaraldehyde / 2% Paraformaldehyde in 0.1M sodium cacodylate buffer (pH 7.4) for 2 hours at RT. Fixative was replaced with 0.1M cacodylate buffer, and samples were post-fixed with 1% Osmiumtetroxide (OsO_4) / 1.5% Potassiumferrocyanide (KFeCN_6) for 1 hour. Subsequently, samples were washed in H_2O three times and incubated in 1% aqueous uranyl acetate for 1 hour followed by 2 washes in H_2O and subsequent dehydration in grades of alcohol (10 minutes each; 50%, 70%, 90%, 2x 10 minutes 100%). The samples were then treated with propyleneoxide for 1 hour and infiltrated overnight in a 1:1 mixture of propyleneoxide and TAAB Epon. The following day, the samples were embedded in TAAB Epon and polymerized at 60°C for 48 hours. Ultrathin sections (60nm) were cut on a Reichert Ultracut-S microtome, picked up onto copper grids stained with lead citrate and examined in a JEOL 1200EX Transmission electron microscope. The TEM images were recorded with an AMT 2k CCD camera.

Statistical Analysis

Triplicate data points were averaged and the mean was graphed unless otherwise indicated. All statistical analyses was performed with the unpaired, two-tailed Student T-

test using GraphPad's - QuickCalcs software, (GraphPad). Statistical significance was set at $P < 0.05$ unless otherwise indicated.

CHAPTER THREE: RESULTS

VEEV infection results in loss of mitochondrial membrane potential and increase in reactive oxygen species

Multiple studies have shown that many viruses including HCV, HIV, RSV, and RVFV produce alterations in mitochondrial membrane potential and increase in oxidative stress in infected cells (Rahmani et al., 2000; Bouchard et al., 2001; Waris et al., 2001; Bouchard and Navas-Martin, 2011; Narayanan et al., 2011; Narayanan et al., 2014). We wanted to determine if VEEV infection will result in a disruption of mitochondrial function in the human astrocytoma cell line, U87MG. We have utilized U87MG cells as a model system in prior studies to understand host responses to New World alphavirus infections (Narayanan et al., 2011; Kehn-Hall et al., 2012; Lundberg et al., 2013; Amaya et al., 2014; Voss et al., 2014; Amaya et al., 2015). Using the live, attenuated vaccine strain, TC-83, as our model, we investigated whether infection of U87MG cells with VEEV will change the mitochondrial membrane potential in a time dependent and multiplicity of infection (MOI) dependent manner.

U87MG cells were infected with TC-83 at MOI: 10 and MOI: 20. Uninfected cells were maintained alongside as controls. All cells were quantified for mitochondrial membrane potential at 2, 4 and 6 hpi by treatment with 1 μ M TMRE (TetraMethyl Rhodamine, Ethyl ester) reagent diluted in complete medium. TMRE is a fluorescent probe which will label active mitochondria by virtue of it being a cell permeable,

positively charged dye with a relative negative charge of the cells. If mitochondria are inactive or depolarized, TMRE will not be readily sequestered, which will be reflected as a decrease in mean fluorescence intensity (Perry et al., 2011). All cells were incubated for 20 minutes with TMRE and maintained at 37°C, after which fluorescence was quantified. These data demonstrated that TC-83 (MOI: 10) infection results in a decrease in membrane potential at 2, 4, and 6 hpi, when compared to the untreated mock cells, and this result was found to be statistically significant ($p \leq 0.05$) at 4 and 6 hpi (Figure 1A). While we observed ~20% drop in membrane potential at 4 hpi, the decrease was further exacerbated with a ~30% drop in membrane potential at 6 hpi, suggesting that the impact on membrane potential was time dependent. The loss in membrane potential was also MOI dependent as evidenced by the outcomes at MOI: 20 (Figure 1B) which was statistically significant ($*p \leq 0.05$) at 4 and 6 hpi (Figure 1B). Comparatively, the higher MOI resulted in ~30% drop in membrane potential at 4 hpi and ~40% drop at 6 hpi. Overall, the results illustrated that TC-83 infection of U87MG cells leads to a decrease in mitochondrial membrane potential in an infectious dose dependent and time dependent manner.

Maintenance of mitochondrial membrane potential is essential for functionality of the respiratory chain and oxidative phosphorylation for ATP production. ROS are signaling molecules that can reflect the membrane potential (Li et al., 1999; Suski et al., 2012). The accumulation of ROS is connected to oxidative stress in many infectious and noninfectious pathological states, such as RVFV, Herpes Virus, aging, and cancer (Narayanan et al., 2011; Liochev, 2013; Santana et al., 2013; Narayanan et al., 2014;

Hikita et al., 2015). Hence, we expected that determination of ROS accumulation, in addition to quantification of the membrane potential, may provide supportive information about the integrity of mitochondrial function.

To that end, we performed microscopy analysis of TC-83 infected U87MG cells using MitoSox stain. MitoSox is a cell-permeating red fluorescent mitochondrial superoxide indicator which can be used to visualize superoxide accumulation in cells and, hence, utilized as a qualitative determination of ROS accumulation (Dagda et al., 2009; Gandhi et al., 2009; Narayanan et al., 2011; Narayanan et al., 2014). U87MG cells were seeded in an 8-well chamber slide and were either uninfected or infected with TC-83 at MOI: 10 and stained at 6 hpi. TC-83 infected cells showed an increased accumulation of ROS at 6 hpi when compared to the uninfected cells (Figure 1C).

Since our microscopy analysis provided only a qualitative measure of ROS accumulation in TC-83 infected cells, as a next step we employed a quantitative method of measuring ROS levels using OxiSelect Intracellular ROS Assay Kit. ROS species react with 2',7'-dichlorodihydrofluorescein (DCFH-DA), a cell-permeable fluorogenic probe, which is rapidly oxidized to the fluorescent 2',7'-dichlorodihydrofluorescein (DCF) (Cell Biolabs Inc., San Diego, CA, USA). Fluorescence intensity is proportional to the total ROS levels within the cell cytosol. U87MG cells were seeded in a 96-well black plate and were either uninfected (mock), infected with TC-83 MOI: 10, or treated with 100 μ M H₂O₂. Cells were pre-incubated for 30 minutes with 1X (1M) DCFH-DA in FBS-free DMEM prior to infection/treatment for 1 hour at 37°C, 5% CO₂. The addition of H₂O₂ to uninfected cells served as a positive control and uninfected mock cells served as

a negative control. Fluorescence was detected at 6 hpi. Two independent experiments were performed in technical triplicates and averaged. Results indicated a 300% increase in ROS in the TC-83 infected cells as compared to the uninfected cells (Figure 1D). Cumulatively, our data supported the loss of membrane potential and accumulation of ROS in U87MG cells following TC-83 infection.

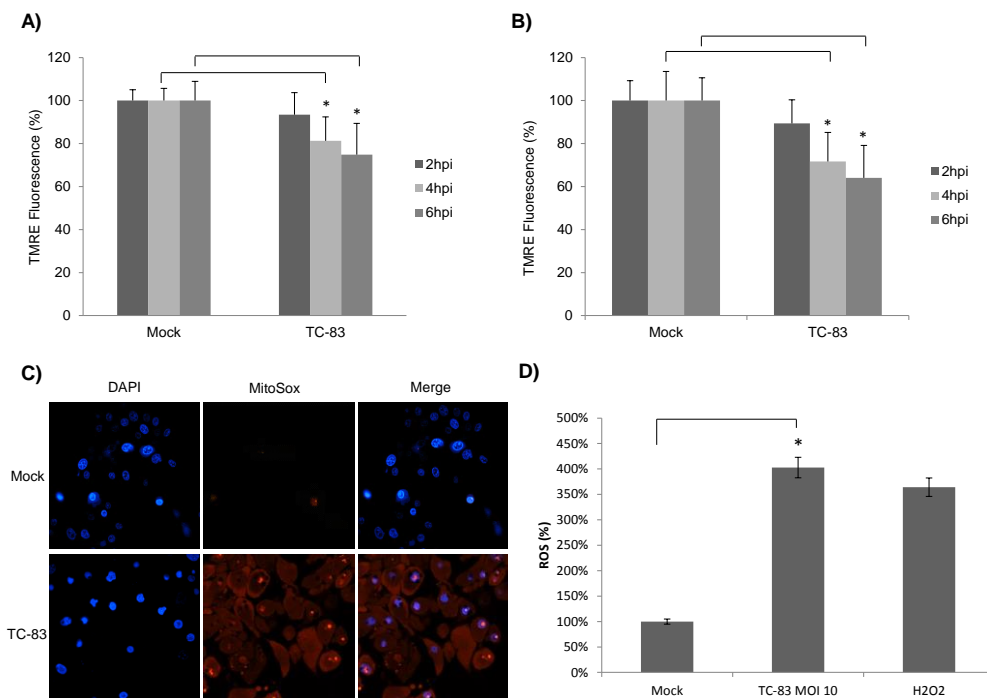


Figure 1: TC-83 infection of U87MG cells resulted in loss of membrane potential and an increase in reactive oxygen species. **A)** U87MG cells were seeded in a 96-well black plate and were either uninfected or infected with TC-83 at MOI: 10 (**A**) and MOI: 20 (**B**). TMRE reagent was added at 2, 4 and 6 hpi and fluorescence was detected using the DTX 880 multimode detector (Beckman Coulter). The addition of FCCP to mock cells served as a positive control and untreated mock cells served as a negative control. **C)** U87MG cells were seeded in an 8-well chamber slide and were either uninfected (Mock) or infected with TC-83 at MOI: 10 and stained at 6 hpi using MitoSox stain and DAPI. Images were taken using Nikon Eclipse TE2000-U with a 60x objective and are representative of triplicate samples within the same experiment. * $p \leq 0.05$. **D)** U87MG cells were seeded in a 96-well black plate and were either uninfected (mock), infected with TC-83 MOI: 10, or treated with 100 μ M H₂O₂. Cells were pre-incubated for 30 minutes with 1X (1M) DCFH-DA in FBS-free DMEM prior to infection/treatment for 1 hour. The addition of H₂O₂ to uninfected cells served as a positive control and uninfected mock cells served as a negative control. Fluorescence was detected at 6 hpi using the DTX 880 multimode detector (Beckman Coulter). Data represents an average of two independent experiments performed with triplicate samples. * $p \leq 0.05$.

Infected cells displayed differences in intracellular mitochondrial location in comparison with uninfected cells.

Viral infections such as those caused by HBV have been shown to cause a perinuclear distribution of mitochondria wherein mitochondria cluster around the nucleus in an infection dependent manner (Kim et al., 2013). A similar redistribution of mitochondria around the nucleus of infected neurons was demonstrated in the case of Herpes Virus infection accompanied by increased concentration of viral tegument proteins around the nucleus (Murata et al., 2000). Interestingly, such a perinuclear clustering phenotype was also observed in fibroblasts obtained from Alzheimer's disease patients suggestive of a relevance to neurodegenerative conditions (Wang et al., 2008). We wanted to determine if VEEV infection resulted in alterations in mitochondrial distribution in infected cells. U87MG cells that were infected with TC-83 (MOI: 20) were fixed at 4 and 6 hpi and immunofluorescence analysis carried out with antibodies to TOMM20 and VEEV-capsid to evaluate mitochondrial distribution specifically in infected cells. The results indicated that the mitochondria in infected cells clustered around the nucleus in 73-75% of the cells that were positive for VEEV-capsid (Figure 2).

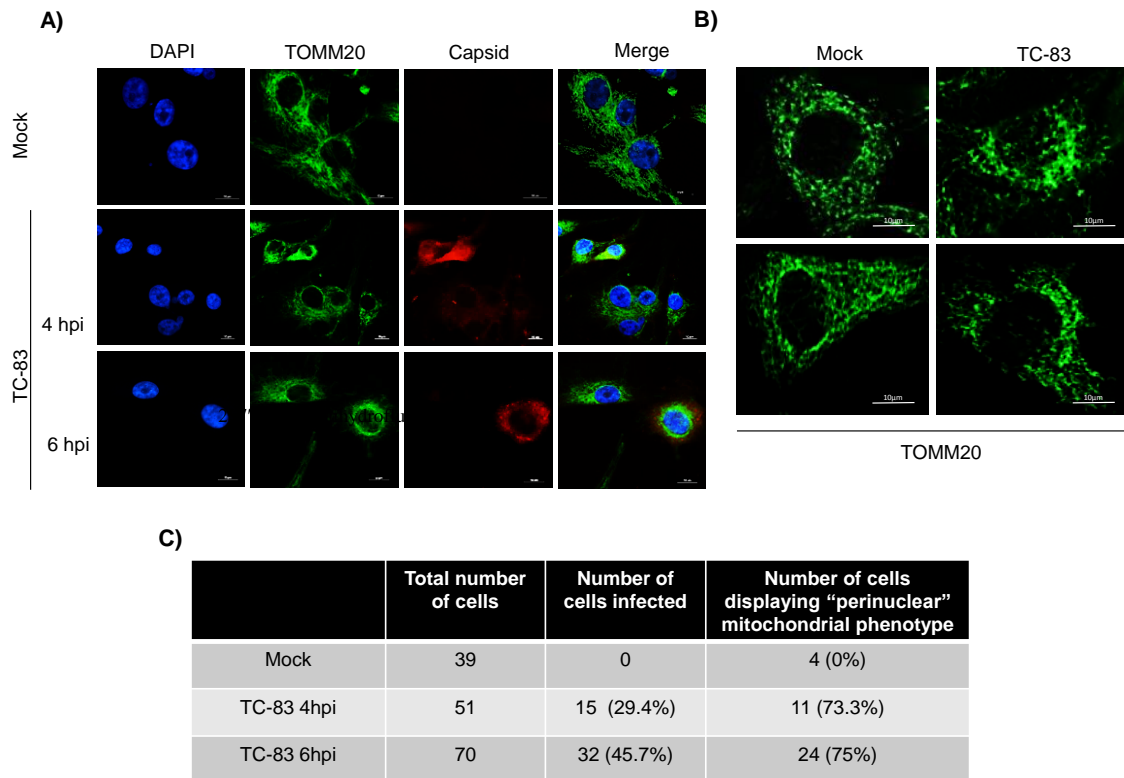


Figure 2: Mitochondria displayed a perinuclear phenotype in TC-83 infected cells. **A)** U87MG cells were seeded in an 8-well chamber slide and were either uninfected (Mock) or infected with TC-83 at MOI: 20. At 4 and 6 hpi, cells were fixed and probed with antibodies to TOMM20 and VEEV capsid with subsequent incubation with Alexa Fluor 488 (green) and 568 (red). The cells were stained with DAPI to observe the nuclei. Images were procured using Nikon Eclipse TE2000-U with a 60x objective and are representative of two independent experiments. **B)** Representative images from A) taken with a 100x objective. **C)** The total number of cells displaying the perinuclear phenotype were tabulated for each sample type.

The VEEV capsid protein was observed to localize in the mitochondria.

Viruses have been known to modulate mitochondrial function by localizing critical virulence factors in the mitochondrial membranes. Perinuclear accumulation of mitochondria in Herpes Virus infection coincided with concentration of viral tegument

protein in a similar pattern as suggested earlier (Murata et al., 2000). Rubella virus, also belonging to the family *Togaviridae*, redistributed mitochondria in infected cells with the capsid protein localizing to mitochondria and contributing to apoptosis (Claus et al., 2011). Rotaviral nonstructural protein 4, a protein known to be involved in apoptosis in infected cells, localized to the mitochondria (Bhowmick et al., 2012). In the case of HBV infections, HBx protein was shown to partly localize to mitochondrial membranes in primary hepatocytes (Clippinger and Bouchard, 2008). Thus, there have been multiple instances in which viral proteins have been documented to localize in mitochondria.

Since other viruses, including the *Togaviridae* family member Rubella virus, have been shown to localize critical virulence factors to the mitochondria (Clippinger and Bouchard, 2008; Claus et al., 2011; Bhowmick et al., 2012), we wanted to determine if VEEV capsid protein displayed any mitochondrial localization. We had utilized capsid signals to verify if a cell was infected or not, as a part of our confocal microscopy analysis of mitochondrial distribution in infected cells. During that analysis, we observed that a part of the capsid signal localized with the mitochondrial TOMM20 signal (Figure 3). In a given infected cell, we were able to observe a partial colocalization of capsid with TOMM20, suggesting that capsid did not show a uniform mitochondrial distribution, but rather, appeared to be sporadic.

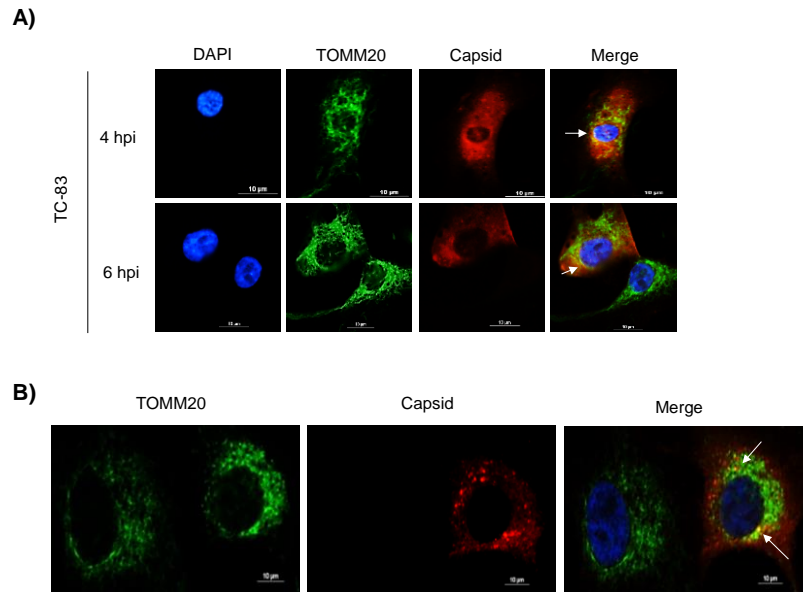


Figure 3: VEEV capsid localized in the mitochondria of infected cells. A) U87MG cells were seeded in an 8-well chamber slide and were either uninfected (Mock) or infected with TC-83 at MOI: 20. At 4 and 6 hpi, cells were fixed and probed with antibodies to TOMM20 and VEEV capsid with subsequent incubation with Alexa Fluor 488 (green) and 568 (red). Images were taken using Nikon Eclipse TE2000-U with a 60x objective. Co-localization of VEEV capsid with TOMM20 (yellow) was observed and shown by the arrows. **B)** Representative images from **A)** shown on a magnified scale.

To determine by an alternate strategy if capsid protein can be seen in association with mitochondrial membranes, we adopted an independent biochemical fractionation method by enriching for mitochondrial membranes. U87MG cells were either uninfected (mock) or infected with TC-83 (MOI: 10 and MOI: 20). Cells were collected at 6 hpi and mitochondrial membrane fractions were separated from the cytosolic fractions. The mitochondrial and cytosolic fractions along with whole cell extracts (WCE) were analyzed by western blot analysis using antibodies to TOMM20, VEEV capsid and β -Actin. As shown in Figure 4A, TOMM20 was significantly enriched in the mitochondrial fraction when compared to the cytosolic fractions (compare lanes 4-6 with 7-9),

indicating that the fractionations were pure. Capsid protein was found to be enriched in the mitochondrial fraction in an infectious dose dependent manner (Figure 4A, compare lanes 5 and 6). Normalized capsid protein band quantification indicated an 83% increase in capsid protein at MOI: 20, whereas at MOI: 10, the capsid protein was quantified to be a 78% increase (Figure 4B). As expected, capsid was also detected in the cytoplasmic fraction (Figure 4A, lanes 8 and 9), while no capsid was detected in the mitochondrial membrane and cytosolic fractions of mock uninfected cells (Figure 4A, lanes 4 and 7). Cumulatively, microscopic and biochemical fractional methods have demonstrated a partial colocalization of capsid protein in infected cells with mitochondrial membranes.

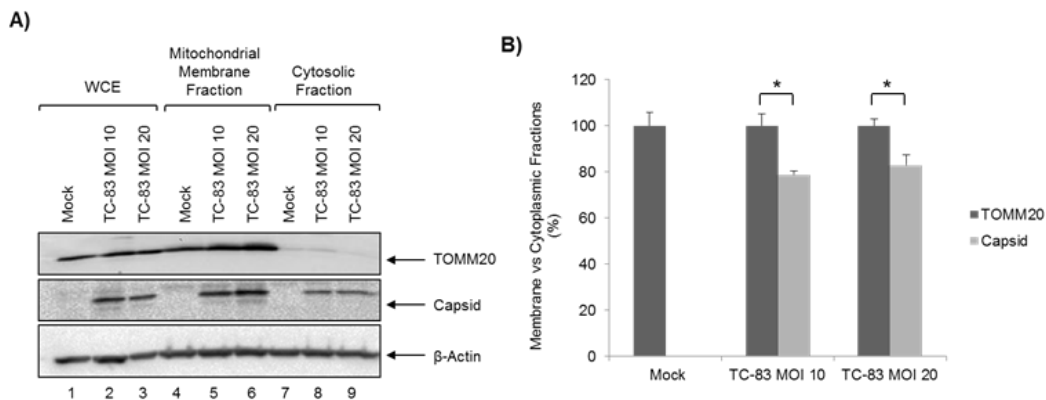


Figure 4. VEEV capsid localized to the mitochondrial membranes of infected cells in an infection dependent manner. **A)** U87MG cells were grown to ~90% confluency in T-225 flasks and were either uninfected (Mock) or infected with TC-83 (MOI: 10, MOI: 20). 2×10^7 cells for each condition were collected at 6 hpi. Mitochondrial membrane and cytosolic fractions were isolated using the Mitochondrial Extraction Kit for Cultured Cells (Thermo Scientific, #89874) according to the manufacturer's instructions. Western blot was performed with whole cell extracts (WCE), mitochondrial membrane and cytosolic fractions to probe for VEEV Capsid. The mitochondrial membrane protein TOMM20 served as a control. **B)** Capsid and TOMM20 concentrations for the mitochondrial membrane fraction were normalized to β -actin. Graph represents protein concentrations of TOMM20 and capsid present in the mitochondrial membrane fraction compared to the total membrane and cytosolic fractions. Data represents three independent experiments. * $p \leq 0.05$.

VEEV capsid co-localized with PINK1 and Parkin in the mitochondrial membrane of TC-83 infected cells.

Viral infection induces alterations in the mitochondrial proteome which includes increased retention of the kinase PINK1 which subsequently recruits Parkin, an E3 ubiquitin ligase. The recruitment of kinase and ubiquitin ligase enzymes to the mitochondria correlate with mitochondrial dysfunction and elimination of defective mitochondria by mitophagy during infectious and noninfectious situations (Gegg et al., 2010; Narendra and Youle, 2011; Okatsu et al., 2012; Kim et al., 2013; Khan et al., 2015). As a next step, we wanted to determine if VEEV capsid colocalizes with PINK1 and Parkin in infected cells. U87MG cells were either uninfected or infected with TC-83 (MOI: 20) and fixed at 6 hpi. Fixed cells were probed with antibodies to PINK1 and VEEV capsid (Figure 5A). Independently, fixed cells were also probed with antibodies to Parkin and VEEV capsid (Figure 5B).

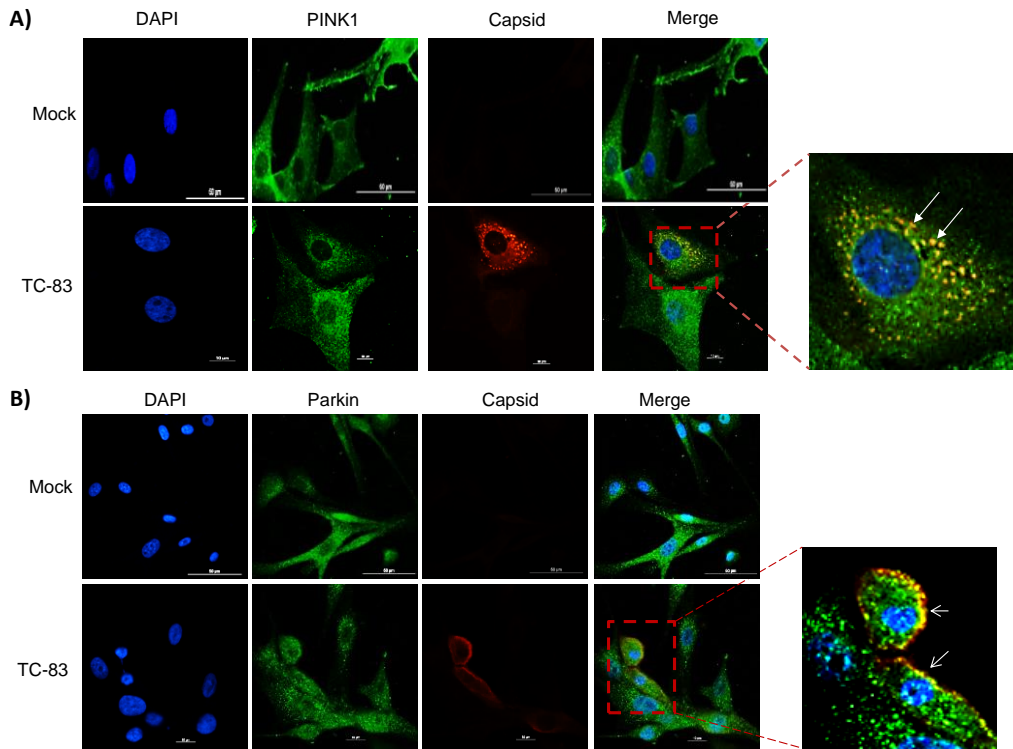


Figure 5: VEEV capsid co-localized with PINK1 and Parkin. **A)** U87MG cells were seeded in an 8-well chamber slide and were uninfected (Mock) or infected with TC-83 at MOI: 20. At 6 hpi, cells were fixed and probed with antibodies to PINK1 and VEEV capsid, with subsequent incubation with Alexa Fluor 488 (green) and 568 (red), respectively. The cells were stained with DAPI to observe the nuclei. Images were taken using Nikon Eclipse TE2000-U with a 60x objective. Co-localization of VEEV capsid with PINK1 (yellow) was observed and shown by the arrows. **B)** U87MG cells were infected with TC-83 at MOI: 20. At 6 hpi, uninfected and infected cells were fixed and probed with antibodies to Parkin and VEEV capsid, with subsequent incubation with Alexa Fluor 488 (green) and 568 (red), respectively. Images were taken using Nikon Eclipse TE2000-U with a 60x objective. Co-localization of VEEV capsid with Parkin (yellow) was observed and shown by the arrows.

Our studies revealed that capsid, which served as an infection control, colocalized with PINK1 and Parkin; however, this outcome does not reveal that the colocalization of capsid with PINK1 and Parkin occurred in the mitochondrial membranes. In order to determine if an increased retention of PINK1 and Parkin could be detected in

mitochondrial membranes, we biochemically enriched mitochondrial membranes and analyzed for PINK1, Parkin, TOMM20 and VEEV capsid by western blot analysis. U87MG cells were infected with increasing concentrations of TC-83 (MOI: 10 and MOI: 20) and collected at 6 hpi. Uninfected cells served as controls. WCE from all samples were also run as controls (Figure 6A, lanes 1-3) and TOMM20, PINK1 and Parkin levels were comparable between uninfected and infected cells. Therefore, even if there were differential enrichment of any of these target proteins in infected cells it was not a result of differential protein expression.

We also independently determined that TC-83 infection did not result in an increase in the total protein levels of PINK1 and Parkin in infected cells. As expected, capsid protein was detected only in WCE obtained from infected cells and increased in an infectious dose dependent manner. TOMM20 was enriched in the mitochondrial membrane fractions in uninfected and infected cells as anticipated (lanes 4-6). Interestingly, PINK1 was enriched in the mitochondrial membrane fractions in an infectious dose dependent manner (Figure 6A, lanes 4-6). Quantification of PINK1 in the mitochondrial membranes, as normalized to β -actin from three independent experiments indicated a statistically significant infectious dose dependent enrichment when compared to the uninfected control (Figure 6B). At the highest MOI tested, there was twice as much PINK1 in the mitochondrial membranes in infected cells when compared to uninfected cells. Similarly, Parkin recruitment to the mitochondrial membranes was increased in infected cells (Figure 6A). Quantification of mitochondrial membrane associated Parkin

from three independent experiments showed the increase to be statistically significant (Figure 6B).

In contrast to PINK1, Parkin could still be detected in the cytosolic fractions of infected cells, which supports the model outlined by Khan et al. (2015) that translocation of PINK1 precedes the recruitment of Parkin to the mitochondrial membrane (Figure 6A, lanes 7-9). Cumulatively, our microscopic and biochemical fractionation studies demonstrated that VEEV infection resulted in colocalization of PINK1 and Parkin with capsid protein. The data also demonstrated relocalization of PINK1 and Parkin to mitochondrial membranes in an infectious dose dependent manner.

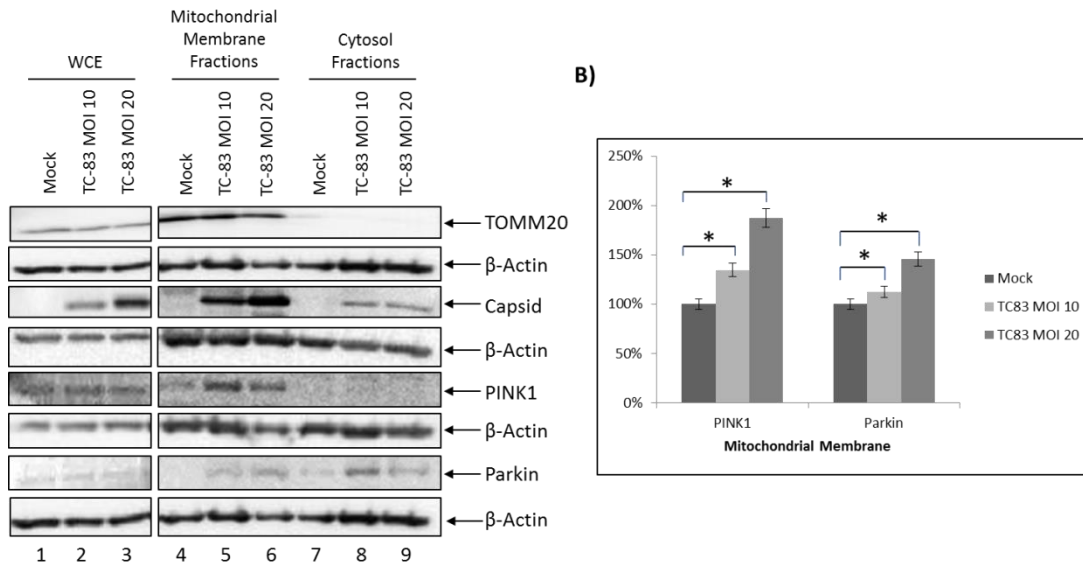
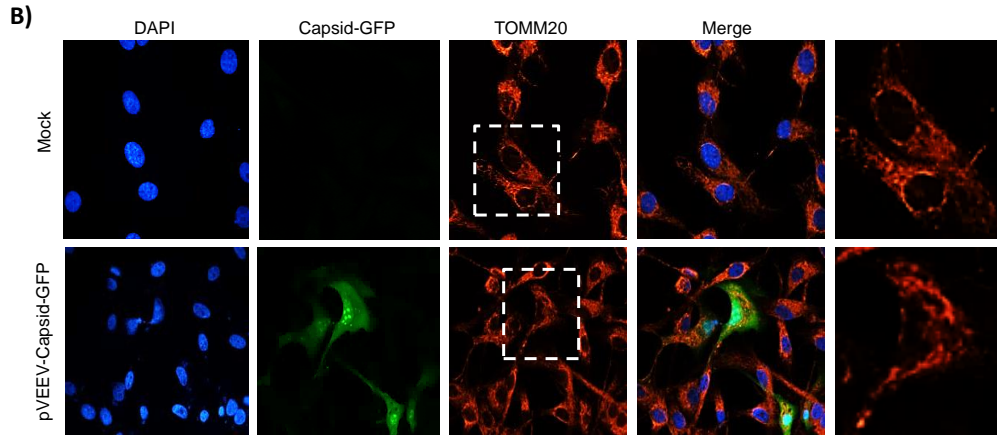
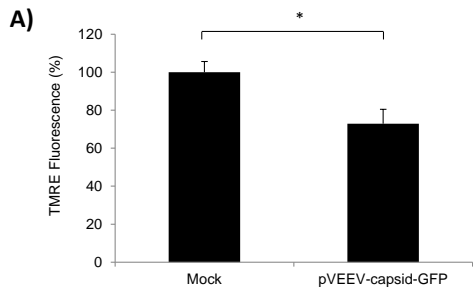


Figure 6. PINK1 and Parkin co-localize in the mitochondrial membrane of TC-83 infected cells.

A) U87MG cells were either uninfected (Mock) or infected with TC-83 MOI 10 or MOI 20 and cells were collected at 6 hpi. Mitochondrial membrane and cytosolic fractions were isolated and western blot was performed with whole cell extracts, mitochondrial membrane and cytoplasmic fractions to probe for VEEV Capsid, PINK1 and Parkin. The mitochondrial membrane protein TOMM20 served as a control. **B)** TOMM20, PINK1 and Parkin concentrations for the mitochondrial membrane fraction were normalized to β -actin. Graph represents protein concentrations of PINK1 and Parkin present in the mitochondrial membrane fraction compared to mock uninfected cells. Data represents three independent experiments. $*p \leq 0.05$.

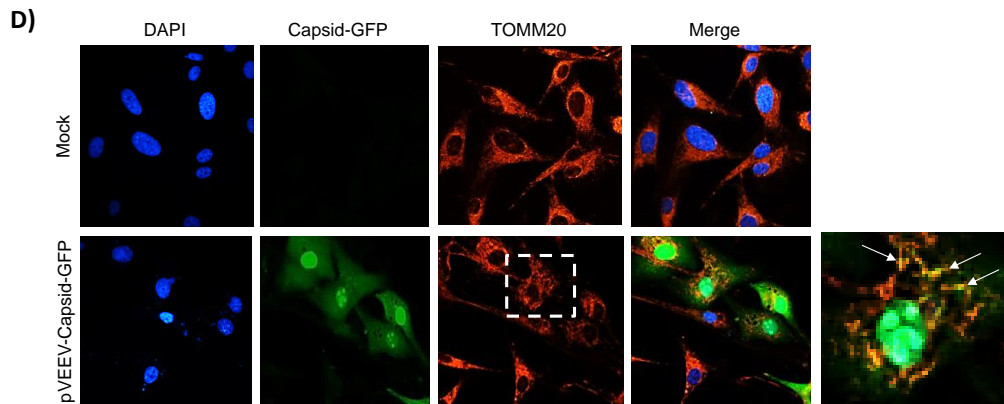
Overexpression of capsid protein resulted in a decrease in mitochondrial membrane potential and altered intracellular distribution.

We wanted to determine if the capsid protein was able to independently induce the altered mitochondrial dynamics, specifically loss of membrane potential and perinuclear distribution. Notably, overexpression of the Influenza A virus protein PB1-F2 led to its relocation to the inner mitochondrial membrane via TOMM40 channels and disrupted membrane potential (Gibbs et al., 2003; Yoshizumi et al., 2014). U87MG cells were transfected with a plasmid construct that expressed capsid as a GFP fusion protein and cells were analyzed for mitochondrial membrane potential at 24 hpi. Quantification of mitochondrial membrane potential using TMRE allowed us to reveal 30% drop in cells that were transfected with the capsid overexpression construct (Figure 7A). Next, we performed microscopic analysis of transfected cells to determine the impact of capsid overexpression on mitochondrial distribution. In cells that expressed GFP-capsid, a modest compacting of mitochondria around the nucleus could be observed, although the tight perinuclear distribution observed in the case of infection was not observed here (Figure 7B). This suggests that the perinuclear clustering phenotype observed in the context of infected cells may also be influenced by other viral components. Finally, overexpressed capsid protein displayed a partial colocalization with TOMM20, mirroring the outcome in infected cells where some mitochondria displayed capsid localization (Figure 7C).



C)

| | Total number of cells | Number of cells displaying GFP | Number of cells displaying "perinuclear" mitochondrial phenotype |
|------------------|-----------------------|--------------------------------|--|
| Mock | 105 | 0 | 5 (0%) |
| pVEEV-capsid-GFP | 116 | 31 (27%) | 18 (58%) |



E)

| | Total number of cells | Number of cells displaying GFP | Number showing co-localization of VEEV capsid with TOMM20 (%) |
|------------------|-----------------------|--------------------------------|---|
| Mock | 112 | 0 | 0 (0%) |
| pVEEV-capsid-GFP | 123 | 51 (41%) | 6 (12%) |

Figure 7. Over expressed VEEV capsid resulted in altered mitochondrial dynamics. **A)** U87MG cells were transfected with VEEV-GFP-Capsid. TMRE reagent was added at 24 hours post transfection and fluorescence was detected using the DTX 880 multimode detector (Beckman Coulter). **B)** U87MG cells were seeded in an 8-well chamber slide and were either not transfected or transfected with VEEV-GFP-Capsid. At 24 hours post transfection, cells were fixed and probed with antibodies to TOMM20, with subsequent incubation with Alexa Fluor 568 (red). The nuclei were visualized by DAPI staining. Images were procured using Nikon Eclipse TE2000-U with a 60x objective. **C)** The total number of cells displaying the perinuclear phenotype is tabulated for each sample type. **D)** U87MG cells that were transfected with VEEV-GFP-Capsid were fixed at 24 hours post transfection and probed with antibodies to TOMM20, with subsequent incubation with Alexa Fluor 568 (red). Images were acquired using Nikon Eclipse TE2000-U with a 60x objective and colocalization of VEEV capsid with TOMM20 (yellow) was observed and shown by the arrows. **E)** Number of cells that display colocalization of capsid with TOMM20 is tabulated.

High resolution imaging of VEEV infected cells demonstrated alterations in mitochondrial structure.

Next, we determined if the mitochondria in TC-83 infected cells displayed any structural alterations when compared to those of uninfected cells. We chose 6 hpi for our analyses, as at this time point we have observed the maximum decrease in membrane potential, perinuclear clustering and altered localization of capsid, PINK1 and Parkin resulting from TC-83 infection. We performed Transmission Electron Microscopy (TEM) analysis of U87MG cells infected with TC-83 virus (MOI: 20) to determine if TC-83 infection led to any structural changes in the mitochondria. Uninfected cells were maintained as negative controls. All cells were fixed at 6 hpi with 2.5% glutaraldehyde / 2% Paraformaldehyde in 0.1 M sodium cacodylate buffer (pH 7.4). Ultra-thin sections were stained with a solution of 1 % uranyl acetate and lead citrate. Sections were examined with a JEOL 1010 transmission electron microscope, and images were recorded with an AMT 2k CCD camera.

In infected cells, the mitochondria displayed a range of abnormalities in structure, including partially swollen mitochondria (Figure 8B). In addition to mitochondria cristae, some of these structures displayed the compacting of internal membrane, with the

separated pieces of membranous structures having no apparent connection to the outer membranes detected (Figure 8C, D). These compact inner structures with a blebbed membrane-like architecture were not detected in uninfected cells (Figure 8A) and appeared larger than the traditional granules. Finally, in some cases, mitochondria displayed a tendency to congregate together in the infected cells (Figure 8E). Thus, cumulatively, our TEM studies revealed that at the ultrastructural level, mitochondria display a range of structural alterations as a result of TC-83 infection.

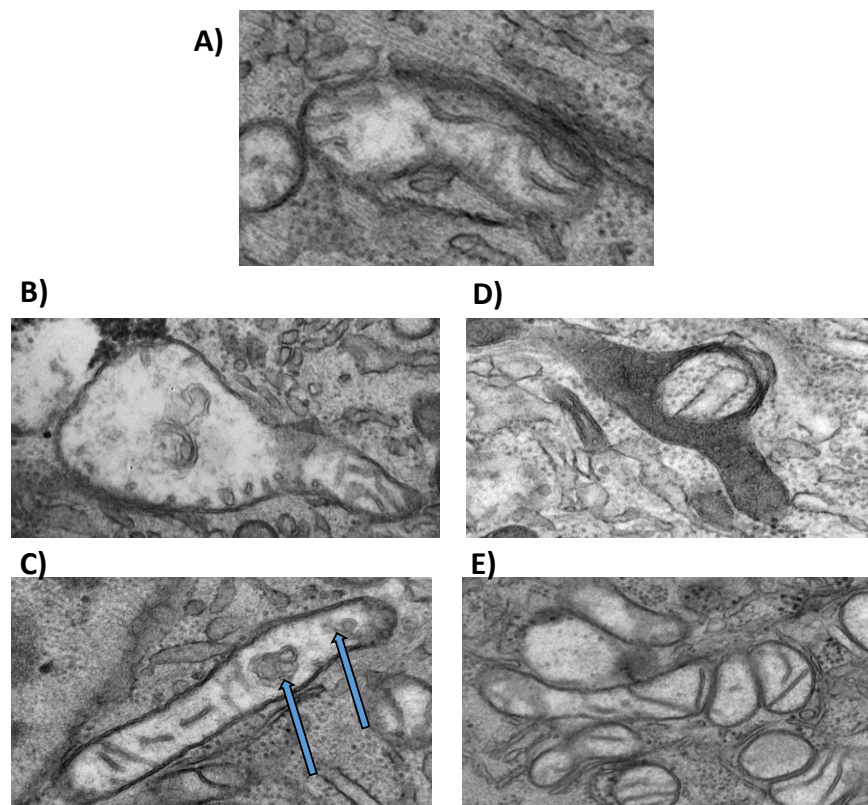


Figure 8. Mitochondria in TC-83 infected cells display morphological alterations. U87MG cells infected with TC-83 (MOI: 20) were fixed at 6 hpi and processed for TEM imaging. Ultrathin sections of 60 nm were made and images of mitochondria obtained at 25000X magnification. (A) Example of mitochondria obtained from an uninfected cell and changes in mitochondrial morphology, such as (B) heterogeneously swollen, (C) and (D) changes to inner mitochondrial membrane (clumped structures inside membrane), and (E) clustering of mitochondria. Images were acquired with a MegaView III digital camera (Olympus).

CHAPTER FOUR: DISCUSSION

New World alphaviruses are encephalitic viruses that produce neuronal outcomes in equines and humans. VEEV infection is well documented to result in CPE in a capsid protein dependent manner (Garmashova et al., 2007; Atasheva et al., 2010; Lundberg et al., 2013). Our focus was on host-based mechanisms involving the mitochondria that may further our understanding of disease progression and potentially explain the CPE phenotype. The mitochondria are sentinel organelles involved in many essential cellular functions including production of energy, innate immune signaling and deciding cellular fate (Ernster and Schatz, 1981; Chan, 2006; McBride et al., 2006; Khan et al., 2015). Mitochondrial membrane potential is a cell type independent indicator of mitochondrial integrity and functional competence. In a healthy cell, membrane potential is maintained due to a functional mitochondrial respiratory chain and oxidative phosphorylation. As a part of the energy production process, ROS is produced in normal cells as well (Devasagayam et al., 2004). However, pathogenic conditions that may result in disruption of mitochondrial membrane potential will impact the integrity of the electron transport chain and result in an abnormal accumulation of ROS. Thus, a deviation in the mitochondrial membrane potential and accumulated ROS are reliable indicators of interruption of mitochondrial function. We have observed an infectious dose dependent and time dependent decrease in mitochondrial membrane potential that is also

accompanied by a prominent increase in ROS in human astrocytoma cells infected with the TC-83 strain of VEEV (Figure 1).

Many viral infections have been recognized as being causative of oxidative stress phenotypes. HIV, particularly in the cases of HIV associated dementia, and acute encephalitis phenotypes resulting from Herpes Virus infections involve prominent onset of oxidative stress (Williams et al., 2010; Santana et al., 2013). The observed changes in mitochondrial membrane potential and ROS accumulation may be early events that set the stage for apoptosis in VEEV infections through the intrinsic pathway.

Notably, this phenotype was observed when cells were infected with the attenuated strain of VEEV, TC-83. TC-83 is plagued by reactogenicity concerns, because of which it is not approved for public use. It may be an important safety consideration to ensure that disruption of mitochondrial function is not associated with the reactogenic phenotype. It will also be of interest that the virulent strains of VEEV, such as Trinidad Donkey (TrD) strain, may result in an exaggerated oxidative stress with different kinetics when compared to the TC-83 strain. Such differences in oxidative stress mechanisms may be early discriminators of virulence that establish kinetics of host inflammatory responses at early times post exposure.

Mitochondrial distribution in cells and mitochondrial mobility is an essential feature of healthy cells. Neuronal cells in particular, are significantly impacted by mitochondrial distribution between the cell body and axon. Anterograde transport of mitochondria in neurons is mediated by kinesin motors on microtubules, while retrograde transport is mediated by dynein motors. In Herpes Virus infections, it was demonstrated

that anterograde transport of mitochondria is disrupted due to impaired association of mitochondria with the kinesin motor (Kramer and Enquist, 2012). This results in severe impairment of mitochondrial mobility in an infection dependent manner. Mitochondrial congregation in a perinuclear manner has been observed in correlation with oxidative stress in many noninfectious neurodegenerative states (Liu et al., 2012). We have observed a prominent perinuclear clustering of mitochondria in TC-83 infected cells (Figure 2). In the context of neurons, this will have a direct impact on neuronal functionality, which may also contribute to neuronal death and encephalitis in VEEV infection.

Viruses often manipulate mitochondrial function by localizing viral proteins in the mitochondrial membranes. Viral proteins have been known to localize to all parts of mitochondria, including outer membrane, inner membrane and mitochondrial lumen (Khan et al., 2014). Localization of viral proteins in mitochondria result in impaired innate immune signaling, in addition to disrupting mitochondrial function (Khan et al., 2014). An excellent example of this phenomenon is Respiratory Syncytial Virus (RSV) nonstructural protein 1 (NS1) which interacted with mitochondrial antiviral signaling protein (MAVS) and interrupted RIG-I based signaling (Boyapalle et al., 2012). Rubella virus is an RNA virus belonging to the family *Togaviridae* whose capsid protein localized to the mitochondria in a manner based on post translational modification (Willows et al., 2014). VEEV capsid protein is associated with onset of CPE in infected cells (Garmashova et al., 2007; Atasheva et al., 2010; Lundberg et al., 2013). We have

observed that a fraction of mitochondria display capsid localization and capsid retention in mitochondrial membranes in an infectious dose dependent manner (Figure 3 and 4).

Of interest to us was the observation that capsid localized with the host kinase PINK1 and ubiquitin ligase Parkin in the mitochondria (Figure 5 and 6). Both PINK1 and Parkin have generated significant interest in recent years in being associated with mitochondrial dysfunction in neurodegeneration. Of direct relevance to mitochondrial motility, PINK1 activity is known to phosphorylate Miro, a connecting link between mitochondria and kinesin. In addition, Parkin ubiquitinates Miro, and ultimately this leads to its degradation. PINK1 is also known to phosphorylate Parkin and contribute to its ubiquitination function (Shiba-Fukushima et al., 2014). Thus, a combined action of phosphorylation and ubiquitination of inherent mitochondrial proteins such as Miro will have a direct impact on mitochondrial intracellular distribution (Wang et al., 2011; Ordureau et al., 2015). Our results are the first demonstration of localization of alphavirus proteins with mitochondrial components in infected cells.

In addition, we have recently demonstrated that VEEV capsid exists in an ubiquitinated state in U87MG cells (Amaya et al., 2015). It would be interesting to determine if capsid protein in mitochondria exists in an ubiquitinated state and if this modification is mediated by Parkin. Indeed, it has been demonstrated that in the case of Rubella virus capsid protein, the phosphorylated form of the viral protein is associated with mitochondrial p32 protein (Beatch and Hobman, 2000; Willows et al., 2014).

Ongoing studies in our laboratory are focused on characterizing the mitochondrial proteomes, including proteins of host or viral origin in VEEV infections. We imagine that

at least a fraction of the proteins that are located in the mitochondria may show differences based on strain virulence. While we observed that overexpression of the capsid protein also produces a comparable decrease in membrane potential (Figure 7), which was similar to that observed in infected cells, the perinuclear clustering phenotype was, to an extent, modest when we overexpressed capsid alone as compared to what was observed in infection. This may be indicative of additional events mediated by other viral components including viral nucleic acids that may exaggerate the mitochondrial distribution profile in early stages of VEEV infection. *In situ* hybridization with VEEV specific probes may be able to shed light on potential involvement of viral RNA on mitochondrial distribution. This is not a far-fetched idea as it was shown with Rubella virus that disruption of stable interactions between viral capsid and host p32 led to a decrease in production of subgenomic RNA and also a decrease in viral titers (Beatch et al., 2005).

At the electron microscopic level, we detected some interesting alterations to the mitochondria at all analyzed timepoints (Figure 8). In a recent publication on mitochondrial changes induced in Parvovirus infection, the authors reported a mitochondrial dysfunction, including a drop in membrane potential and accumulation of ROS (Nykyk et al., 2014). The authors provided electron microscopic visuals of abnormal mitochondrial phenotypes that look very similar to the ones we have presented above, including heterogeneously swollen mitochondria, membrane blebbing and disappearance of cristae (Nykyk et al., 2014). Notably, the authors indicated activation of MEK/ERK signaling resulting from mitochondrial dysfunction in Parvovirus infection.

These events occurred early in infection (2-4 hpi), and therefore were found to be important to the establishment of Parvovirus infection. The authors also found that inhibition of ERK1/2 resulted in reduced membrane depolarization. We have previously demonstrated that VEEV infection leads to robust activation of the MEK/ERK signaling cascade, which is important for the virus to establish a productive infection (Voss et al., 2014). In the case of HCV infected cells, similar clustering of mitochondria was demonstrated (Chu et al., 2011). In HIV infected cells, mitochondria displayed morphological alterations, including disappearance of cristae (Sasaki et al., 2002).

Taken together, our data suggest that VEEV infection produces a significant impact on mitochondrial dynamics in infected cells. The onset of mitochondrial dysfunction during the early stages of VEEV infection may set the stage for downstream events that culminate in neuronal death. Mitochondrial dysfunction may be associated in a cause and effect manner with pronounced alterations to the mitochondrial proteome, a deeper understanding of which will shed more light on the mitochondrial influence on disease progression in New World alphavirus infections.

REFERENCES

- Amaya, M., Voss, K., Sampey, G., Senina, S., de la Fuente, C., Mueller, C., Calvert, V., Kehn-Hall, K., Carpenter, C., Kashanchi, F., Bailey, C., Mogelsvang, S., Petricoin, E., & Narayanan, A. (2014). The role of IKK β in Venezuelan equine encephalitis virus infection. *PloS One* 9, e86745. doi: 10.1371/journal.pone.0086745.
- Amaya, M., Keck, F., Lindquist, M., Voss, K., Scavone, L., Kehn-Hall, K., Roberts, B., Bailey, C., Schmaljohn, C., & Narayanan, A. (2015). The ubiquitin proteasome system plays a role in Venezuelan equine encephalitis virus infection. *PloS One* 10, e0124792. doi: 10.1371/journal.pone.0124792.
- Atasheva, S., Krendelchtchikova, V., Liopo, A., Frolova, E., & Frolov, I. (2010). Interplay of acute and persistent infections caused by Venezuelan equine encephalitis virus encoding mutated capsid protein. *J. Virol.* 84, 10004–10015. doi: 10.1128/JVI.01151-10.
- Atasheva, S., Fish, A., Fornerod, M., & Frolova, E.I. (2010). Venezuelan equine Encephalitis virus capsid protein forms a tetrameric complex with CRM1 and importin alpha/beta that obstructs nuclear pore complex function. *J. Virol.* 84, 4158–4171. doi: 10.1128/JVI.02554-09.
- Atasheva, S., Kim, D.Y., Frolova, E.I., & Frolov, I. (2015). Venezuelan equine encephalitis virus variants lacking transcription inhibitory functions demonstrate highly attenuated phenotype. *J. Virol.* 89, 71–82. doi: 10.1128/JVI.02252-14.
- Barber, T.L., Walton, T.E., & Lewis, K.J. (1978). Efficacy of trivalent inactivated encephalomyelitis virus vaccine in horses. *Am. J. Vet. Res.* 4, 621-5.
- Beatch, M.D. & Hobman, T.C. (2000). Rubella virus capsid associates with host cell protein p32 and localizes to mitochondria. *J. Virol.* 74, 5569–5576.
- Beatch, M.D., Everitt, J.C., Law, L.J., & Hobman T.C. (2005). Interactions between rubella virus capsid and host protein p32 are important for virus replication. *J. Virol.* 79, 10807–10820. doi: 10.1128/JVI.79.16.10807-10820.2005.

- Bhowmick, R., Halder, U.C., Chattopadhyay, S., Chanda, S., Nandi, S., Bagchi, P., Nayak, M.K., Chakrabarti, O., Kobayashi, N., & Chawla-Sarkar, M. (2012). Rotaviral enterotoxin nonstructural protein 4 targets mitochondria for activation of apoptosis during infection. *J. Biol. Chem.* 287, 35004–35020. doi: 10.1074/jbc.M112.369595.
- Bouchard, M.J., Wang, L.H., & Schneider, R.J. (2001). Calcium signaling by HBx protein in hepatitis B virus DNA replication. *Science* 294, 2376–2378.
- Bouchard, M.J. & Navas-Martin, S. (2011). Hepatitis B and C virus hepatocarcinogenesis: lessons learned and future challenges. *Cancer Lett.* 305, 123–143. doi: 10.1016/j.canlet.2010.11.014.
- Boyapalle, S., Wong, T., Garay, J., Teng, M., San Juan-Vergara, H., Mohapatra, S., & Mohapatra, S. (2012). Respiratory syncytial virus NS1 protein colocalizes with mitochondrial antiviral signaling protein MAVS following infection. *PloS One* 7, e29386. doi: 10.1371/journal.pone.0029386.
- Chan, D.C. (2006). Mitochondria: dynamic organelles in disease, aging, and development. *Cell* 125, 1241–1252. doi:10.1016/j.cell.2006.06.010.
- Chu, V.C., Bhattacharya, S., Nomoto, A., Lin, J., Zaidi, S.K., Oberley, T.D., Weinman, S.A., Azhar, S., & Huang, T.-T. (2011). Persistent expression of hepatitis C virus non-structural proteins leads to increased autophagy and mitochondrial injury in human hepatoma cells. *PloS One* 6, e28551. doi: 10.1371/journal.pone.0028551.
- Claus, C., Chey, S., Heinrich, S., Reins, M., Richardt, B., Pinkert, S., Fechner, H., Gaunitz, F., Schäfer, I., Seibel, P., Liebert, U.G. (2011). Involvement of p32 and microtubules in alteration of mitochondrial functions by rubella virus. *J. Virol.* 85, 3881–3892. doi: 10.1128/JVI.02492-10.
- Clippinger, A.J. & Bouchard, M.J. (2008). Hepatitis B virus HBx protein localizes to mitochondria in primary rat hepatocytes and modulates mitochondrial membrane potential. *J. Virol.* 82, 6798–6811. doi: 10.1128/JVI.00154-08.
- Dagda, R.K., Cherra, S.J., Kulich, S.M., Tandon, A., Park, D., & Chu, C.T. (2009). Loss of PINK1 function promotes mitophagy through effects on oxidative stress and mitochondrial fission. *J. Biol. Chem.* 284, 13843–13855. doi: 10.1074/jbc.M808515200.
- Detmer, S.A. & Chan, D.C. (2007). Functions and dysfunctions of mitochondrial dynamics. *Nat. Rev. Mol. Cell Biol.* 8, 870–879. doi:10.1038/nrm2275.

- Devasagayam, T., Tilak, J.C., Bloor, K.K., Sane Ketaki, S., Ghaskadbi Saroj, S., & Lele, R.D. (2004). Free radicals and antioxidants in human health: current status and future prospects. *J. Assoc. Phys. India* 52, 796.
- Ernster, L. & Schatz, G. (1981). Mitochondria: a historical review. *J. Cell Biol.* 91, 227s–255s.
- Gandhi, S., Wood-Kaczmar, A., Yao, Z., Plun-Favreau, H., Deas, E., Klupsch, K., Downward, J., Latchman, D.S., Tabrizi, S.J., Wood, N.W., Duchon, M.R., & Abramov, A.Y. (2009). PINK1-associated Parkinson's disease is caused by neuronal vulnerability to calcium-induced cell death. *Mol. Cell.* 33, 627–638. doi: 10.1016/j.molcel.2009.02.013.
- Garmashova, N., Atasheva, S., Kang, W., Weaver, S.C., Frolova, E., & Frolov, I. (2007). Analysis of Venezuelan equine encephalitis virus capsid protein function in the inhibition of cellular transcription. *J. Virol.* 81, 13552–13565. doi: 10.1128/JVI.01576-07.
- Gegg, M.E., Cooper, J.M., Chau, K.-Y., Rojo, M., Schapira, A.H.V., & Taanman, J.-W. (2010). Mitofusin 1 and mitofusin 2 are ubiquitinated in a PINK1/parkin-dependent manner upon induction of mitophagy. *Hum. Mol. Genet.* 19, 4861–4870. doi:10.1093/hmg/ddq419.
- Gibbs, J.S., Malide, D., Hornung, F., Bennink, J.R., & Yewdell, J.W. (2003). The influenza A virus PB1-F2 protein targets the inner mitochondrial membrane via a predicted basic amphipathic helix that disrupts mitochondrial function. *J. Virol.* 77, 7214–7224. doi: 10.1128/JVI.77.13.7214-7224.2003.
- Hikita, H., Kodama, T., Tanaka S., Saito, Y., Nozaki, Y., Nakabori, T., Shimizu, S., Hayashi, Y., et al. (2015). Activation of the mitochondrial apoptotic pathway produces reactive oxygen species and oxidative damage in hepatocytes that contribute to liver tumorigenesis. *Cancer Prev. Res. (Phila).* 8, 693-701. Doi: 10.1158/1940-6207.
- Johnson, B.J., Kinney, R.M., Kost, C.L., & Trent, D.W. (1986). Molecular determinants of alphavirus neurovirulence: nucleotide and deduced protein sequence changes during attenuation of Venezuelan equine encephalitis virus. *J. Gen. Virol.* 67 (Pt 9), 1951–1960. doi:10.1099/0022-1317-67-9-1951.

- Kehn-Hall, K., Narayanan, A., Lundberg, L., Sampey, G., Pinkham, C., Guendel, I., Van Duyne, R., Senina, S., Schultz, K.L., Stavale, E., Aman, M.J., Bailey, C., & Kashanchi, F. (2012). Modulation of GSK-3 β activity in Venezuelan equine encephalitis virus infection. *PloS One* 7, e34761. doi: 10.1371/journal.pone.0034761.
- Khan, M., Syed, G.H., Kim, S.-J., & Siddiqui, A. (2015). Mitochondrial dynamics and viral infections: A close nexus. *Biochim. Biophys. Acta.* 1853, 2822–2833. doi:10.1016/j.bbamcr.2014.12.040.
- Kim, S.-J., Syed, G.H., & Siddiqui, A. (2013). Hepatitis C virus induces the mitochondrial translocation of Parkin and subsequent mitophagy. *PLoS Pathog.* 9, e1003285. doi:10.1371/journal.ppat.1003285.
- Kim, S.-J., Khan, M., Quan, J., Till, A., Subramani, S., & Siddiqui, A. (2013). Hepatitis B virus disrupts mitochondrial dynamics: induces fission and mitophagy to attenuate apoptosis. *PLoS Pathog* 9, e1003722. doi:10.1371/journal.ppat.1003722.
- Kim, S.-J., Syed, G.H., Khan, M., Chiu, W.-W., Sohail, M.A., Gish, R.G., & Siddiqui, A. (2014). Hepatitis C virus triggers mitochondrial fission and attenuates apoptosis to promote viral persistence. *Proc. Natl. Acad. Sci. U. S. A.* 111, 6413–6418. doi:10.1073/pnas.1321114111.
- Kinney, R.M., Johnson, B.J., Welch, J.B., Tsuchiya, K.R., & Trent, D.W. (1989). The full-length nucleotide sequences of the virulent Trinidad donkey strain of Venezuelan equine encephalitis virus and its attenuated vaccine derivative, strain TC-83. *Virology* 170, 19–30.
- Kinney, R.M., Chang, G.J., Tsuchiya, K.R., Sneider, J.M., Roehrig, J.T., Woodward, T.M., & Trent, D.W. (1993). Attenuation of Venezuelan equine encephalitis virus strain TC-83 is encoded by the 5'-noncoding region and the E2 envelope glycoprotein. *J Virol* 67, 1269–1277.
- Kramer, T. & Enquist, L.W. (2012). Alphaherpesvirus infection disrupts mitochondrial transport in neurons. *Cell Host Microbe* 11, 504–514. doi:10.1016/j.chom.2012.03.005.
- Li, P-F., Dietz, R., & von Harsdorf, R. (1999). p53 regulates mitochondrial membrane potential through reactive oxygen species and induces cytochrome *c*-independent apoptosis blocked by Bcl-2. *EMBO* 18(21), 6027-6036.
- Liochev, S.I. (2013). Reactive oxygen species and the free radical theory of aging. *Free Radic. Biol. Med.* 60, 1-4. doi: 10.1016/j.freeradbiomed.2013.02.011.

- Liu, S., Sawada, T., Lee, S., Yu, W., Silverio, G., Alapatt, P., Millan, I., Shen, A., Saxton, W., Kanao, T., Takahashi, R., Hattori, N., Imai, Y., & Lu, B. (2012). Parkinson's disease-associated kinase PINK1 regulates Miro protein level and axonal transport of mitochondria. *PLoS Genet.* 8, e1002537. doi:10.1371/journal.pgen.1002537.
- Lundberg, L., Pinkham, C., Baer, A., Amaya, M., Narayanan, A., Wagstaff, K.M., Jans, D.A., & Kehn-Hall, K. (2013). Nuclear import and export inhibitors alter capsid protein distribution in mammalian cells and reduce Venezuelan Equine Encephalitis Virus replication. *Antiviral Res.* 100, 662–672. doi:10.1016/j.antiviral.2013.10.004.
- McBride, H.M., Neuspiel, M., & Wasiak, S. (2006). Mitochondria: more than just a powerhouse. *Curr. Biol.* CB 16: R551–560. doi:10.1016/j.cub.2006.06.054.
- Murata, T., Goshima, F., Daikoku, T., Inagaki-Ohara, K., Takakuwa, H., Kato, K., & Nishiyama, Y. (2000). Mitochondrial distribution and function in herpes simplex virus-infected cells. *J. Gen. Virol.* 81, 401–406. doi:10.1099/0022-1317-81-2-401.
- Narayanan, A., Popova, T., Turell, M., Kidd, J., Chertow, J., Popov, S.G., Bailey, C., Kashanchi, F., & Kehn-Hall, K. (2011). Alteration in superoxide dismutase 1 causes oxidative stress and p38 MAPK activation following RVFV infection. *PloS One* 6, e20354. doi:10.1371/journal.pone.0020354.
- Narayanan, A., Amaya, M., Voss, K., Chung, M., Benedict, A., Sampey, G., Kehn-Hall, K., Luchini, A., Liotta, L., Bailey, C., Kumar, A., Bavari, S., Hakami, R.M., & Kashanchi, F. (2014). Reactive oxygen species activate NFκB (p65) and p53 and induce apoptosis in RVFV infected liver cells. *Virology* 449, 270–286. doi:10.1016/j.virol.2013.11.023.
- Narendra, D.P. & Youle, R.J. (2011). Targeting mitochondrial dysfunction: role for PINK1 and Parkin in mitochondrial quality control. *Antioxid. Redox Signal* 14, 1929–1938. doi:10.1089/ars.2010.3799.
- Nykky, J., Vuento, M., & Gilbert, L. (2014). Role of mitochondria in parvovirus pathology. *PloS One* 9, e86124. doi:10.1371/journal.pone.0086124.
- Okatsu, K., Oka, T., Iguchi, M., Imamura, K., Kosako, H., Tani, N., Kimura, M., Go, E., Koyano, F., Funayama, M., Shiba-Fukushima, K., Sato, S., Shimizu, H., Fukunaga, Y., Taniguchi, H., Komatsu, M., Hattori, N., Mihara, K., Tanaka, K., & Matsuda, N. (2012). PINK1 autophosphorylation upon membrane potential dissipation is essential for Parkin recruitment to damaged mitochondria. *Nat. Commun.* 3, 1016. doi:10.1038/ncomms2016.

- Ordureau, A., Heo, J.-M., Duda, D.M., Paulo, J.A., Olszewski, J.L., Yanishevski, D., Rinehart, J., Schulman, B.A., & Harper, J.W. (2015). Defining roles of PARKIN and ubiquitin phosphorylation by PINK1 in mitochondrial quality control using a ubiquitin replacement strategy. *Proc. Natl. Acad. Sci. U. S. A.* 112, 6637–6642. doi:10.1073/pnas.1506593112.
- Paessler, S. & Weaver, S.C. (2009). Vaccines for Venezuelan equine encephalitis. *Vaccine* 27(Suppl 4), D80–85. doi:10.1016/j.vaccine.2009.07.095.
- Perry, S.W., Norman, J.P., Barbieri, J., Brown, E.B., & Gelbard, H.A. (2011). Mitochondrial membrane potential probes and the proton gradient: a practical usage guide. *BioTechniques* 50, 98-115.
- Rahmani, Z., Huh, K.W., Lasher, R., & Siddiqui, A. (2000). Hepatitis B virus X protein colocalizes to mitochondria with a human voltage-dependent anion channel, HVDAC3, and alters its transmembrane potential. *J. Virol.* 74, 2840–2846.
- Santana, S., Sastre, I., Recuero, M., Bullido, M.J., & Aldudo, J. (2013). Oxidative stress enhances neurodegeneration markers induced by herpes simplex virus type 1 infection in human neuroblastoma cells. *PloS One* 8, e75842. doi:10.1371/journal.pone.0075842.
- Sasaki, M., Miyazaki, K., Koga, Y., Kimura, G., Nomoto, K., & Yoshida, H. (2002). Calcineurin-dependent mitochondrial disturbances in calcium-induced apoptosis of human immunodeficiency virus gp160-expressing CD4+ cells. *J. Virol.* 76, 416–420.
- Shiba-Fukushima, K., Inoshita, T., Hattori, N., & Imai, Y. (2014). PINK1-mediated phosphorylation of Parkin boosts Parkin activity in *Drosophila*. *PLoS Genet.* 10, e1004391. doi:10.1371/journal.pgen.1004391.
- Su, B., Wang, X., Zheng, L., Perry, G., Smith, M.A., & Zhu, X. (2010). Abnormal mitochondrial dynamics and neurodegenerative diseases. *Biochim. Biophys. Acta.* 1802, 135–142. doi:10.1016/j.bbadis.2009.09.013.
- Suen, D-F., Norris, K.L., & Youle, R.J. (2008). Mitochondrial dynamics and apoptosis. *Genes & Development.* 22(12), 1577-1590.
- Suski, J.M., Lebiezinska, M., Bonora, M., Pinton, P., Duszynski, J., & Wieckowski, M.R. (2012). Relation between mitochondrial membrane potential and ROS formation. *Methods Mol. Biol.* 810, 183-205. doi: 10.1007/978-1-61779-382-0_12.

- Taylor, K.G. & Paessler, S. (2013). Pathogenesis of Venezuelan equine encephalitis. *Vet. Microbiol.* 167, 145–150. doi:10.1016/j.vetmic.2013.07.012.
- Terasaki, K., Won, S., & Makino, S. (2013). The C-terminal region of Rift Valley fever virus NSm protein targets the protein to the mitochondrial outer membrane and exerts antiapoptotic function. *J Virol.* 87, 676–682. doi:10.1128/JVI.02192-12.
- Voss, K., Amaya, M., Mueller, C., Roberts, B., Kehn-Hall, K., Bailey, C., Petricoin III, E., & Narayanan, A. (2014). Inhibition of host extracellular signal-regulated kinase (ERK) activation decreases new world alphavirus multiplication in infected cells. *Virology* 468-470, 490–503. doi:10.1016/j.virol.2014.09.005.
- Wang, X., Su, B., Fujioka, H., & Zhu, X. (2008). Dynamin-like protein 1 reduction underlies mitochondrial morphology and distribution abnormalities in fibroblasts from sporadic Alzheimer's disease patients. *Am. J. Pathol.* 173, 470–482. doi:10.2353/ajpath.2008.071208.
- Wang, X., Winter, D., Ashrafi, G., Schlehe, J., Wong, Y.L., Selkoe, D., Rice, S., Steen, J., LaVoie, M.J., & Schwarz, T.L. (2011). PINK1 and Parkin target Miro for phosphorylation and degradation to arrest mitochondrial motility. *Cell* 147, 893–906. doi: 10.1016/j.cell.2011.10.018.
- Waris, G., Huh, K.W., & Siddiqui, A. (2001). Mitochondrially associated hepatitis B virus X protein constitutively activates transcription factors STAT-3 and NF-kappa B via oxidative stress. *Mol Cell. Biol* 21, 7721–7730. doi:10.1128/MCB.21.22.7721-7730.2001.
- Weaver, S.C. (2005). Host range, amplification and arboviral disease emergence. *Arch. Virol. Suppl.* 33–44.
- Weaver, S.C., Ferro, C., Barrera, R., Boshell, J., & Navarro, J.-C. (2004). Venezuelan equine encephalitis. *Annu. Rev. Entomol.* 49, 141–174. doi:10.1146/annurev.ento.49.061802.123422.
- Weaver, S.C., Salas, R., Rico-Hesse, R., Ludwig, G.V., Oberste, M.S., Boshell, J., & Tesh, R.B. (1996). Re-emergence of epidemic Venezuelan equine encephalomyelitis in South America. *VEE Study Group, Lancet Lond. Engl.* 348, 436–440.
- Williams, R., Yao, H., Peng, F., Yang, Y., Bethel-Brown, C., & Buch, S. (2010). Cooperative induction of CXCL10 involves NADPH oxidase: Implications for HIV dementia. *Glia* 58, 611–621. doi:10.1002/glia.20949.

Willows, S., Ilkow, C.S., & Hobman, T.C. (2014). Phosphorylation and membrane association of the Rubella virus capsid protein is important for its anti-apoptotic function. *Cell. Microbiol.* 16: 1201–1210. doi:10.1111/cmi.12272.

Yoshizumi, T., Ichinohe, T., Sasaki, O., Otera, H., Kawabata, S., Mihara, K., & Koshiba, T. (2014). Influenza A virus protein PB1-F2 translocates into mitochondria via Tom40 channels and impairs innate immunity. *Nat. Commun.* 5, 4713. doi:10.1038/ncomms5713.

BIOGRAPHY

Taryn Brooks-Faulconer graduated from Bishop Hoban High School, Wilkes-Barre, Pennsylvania in 1974. Prior to moving to Virginia, she studied Psychology, Anthropology and Geology at UCLA while working as a Paralegal & Secretarial Supervisor at the Intellectual Property Law Firm of Fulwider Patton Lee & Utecht in Los Angeles, California. She received concurrent Bachelor of Science degrees in Biology and Psychology from George Mason University in 2014, graduating Magna cum Laude with honors in both majors. She was employed as a graduate teaching assistant at George Mason for two years, while earning a Master of Science in Biology, with a concentration in Microbiology and Infectious Diseases from George Mason University in 2016.